Supporting Information (SI-2): "Detection and long-term quantification of methane emissions from an active landfill"

Pramod Kumar[1], Christopher Caldow[1,2], Grégoire Broquet[1], Adil Shah[1], Olivier Laurent[1], Camille Yver-Kwok[1], Sebastien Ars[3], Sara Defratyka[1,6], Susan Gichuki[1], Luc Lienhardt[1], Mathis Lozano[1], Jean-Daniel Paris[1], Felix Vogel[3], Caroline Bouchet[4], Elisa Allegrini[4], Robert Kelly[4], Catherine Juery[5], and Philippe Ciais[1]

[1]Laboratoire des Sciences du Climat et de l'Environnement (LSCE/IPSL), CEA-CNRS-UVSQ, Université Paris-Saclay, 91191 Gif-sur-Yvette, France
[2]Climate Science Centre, CSIRO Oceans and Atmosphere, Aspendale, VIC, 3195, Australia
[3]Climate Research Division, Environment and Climate Change Canada, Toronto M3H 5T4, Ontario, Canada
[4]SUEZ-Smart & Environmental Solutions, Tour CB21/16 place de l'Iris, 92040, La Défense, France
[5]TotalEnergies Laboratoire Qualité de l'Air (LQA), 69360 Solaize Cedex, France
[6]now at University of Edinburgh, United Kingdom and National Physical Laboratory, United Kingdom

Correspondence: Pramod Kumar (pramod.kumar@lsce.ipsl.fr)

Abstract. This supporting information material (SI-2) documents the inversion results form different Butte-Bellot campaigns.

Contents

List of Figures

S2.1 Gaussian plume dispersion model

A Gaussian plume model formulates a gas concentration $C(X,Y,Z)$ at the coordinates (X,Y,Z) (for positive X and Z), corresponding to the plume from a point source whose effective release is located at (0, 0, z_{eff}) with release rate q as:

$$C(X,Y,Z) = \frac{Q_s}{2\pi\sigma_Y\sigma_Z U_{eff}} \exp\left(-\frac{Y^2}{2\sigma_Y^2}\right)\left[\exp\left(-\frac{(Z-z_{eff})^2}{2\sigma_Z^2}\right) + \exp\left(-\frac{(Z+z_{eff})^2}{2\sigma_Z^2}\right)\right] \tag{S2.1}$$

where z_{eff} is the effective source height above the ground surface, U_{eff} is the effective mean wind speed at z_{eff} and σ_Y and σ_Z are dispersion coefficients in Y and Z directions, respectively.

In the campaigns whenever the high-frequency measurements from a 3D Sonic anemometer were available, σ_Y and σ_Z are derived from the standard deviations of the corresponding velocity fluctuations in the lateral (σ_v) and the vertical (σ_w) directions as follows (Gryning et al., 1987):

$$\sigma_Y = \sigma_v t\left(1+\sqrt{\frac{t}{2T_Y}}\right)^{-1} \tag{S2.2a}$$

$$\sigma_Z = \sigma_w t\left(1+\sqrt{\frac{t}{2T_Z}}\right)^{-1} \tag{S2.2b}$$

where $t(=X/U_{eff})$ is the travel time from origin to X, and T_Y and T_Z are the Lagrangian time scales in Y and Z directions, respectively. We take $T_Y = 200$ s (Draxler, 1976) for near-surface release and $T_z = 300$ s for unstable conditions $(L<0)$ (Gryning et al., 1987), where L is the Obukhov length. When the high frequency measurements from 3D Sonic anemometer were not available in four campaigns, the Briggs dispersion formulas for flat terrain (Briggs, 1973) based on Pasquill-Gifford-Turner (PGT) stability classes were used to parameterize σ_Y and σ_Z in the Gaussian model. The PGT stability classes were approximately defined based on the magnitude of the wind speed and cloud cover information from the Melun met station. In these four campaigns, the mean wind direction is approximately taken as a direction from the center of the landfill to the location of the maximum averaged CH_4 mole fraction.

S2.1.1 Adaptation of Gaussian model to area sources

Note that the formulation of the Gaussian plume model in Eqs. (S2.1)-(S2.2) is suitable for dispersion of plumes from a point source. To model plumes from the area sources with significant extents compared to the distance to the measurement locations, we adapted two simple formulations of the Gaussian model.

(a) Method-1: based on a modified σ_Y

In this very simple formulation of the Gaussian model for an area source, we modified the total plume spread in the lateral direction σ_Y using the size of an area source. This concept is same as the one has been used when simulating plume dispersion from stacks with significant diameters (Korsakissok and Mallet, 2009). Following this concept, σ_Y (Eq. (S2.2a)) is modified to the total plume "width" as a sum of the plume spread due to turbulence (parameterized following Eq. (S2.2a)) and of the additional initial spread due to the source size which is approximated by the diameter (d_s) of a circular disk centered on the area source and with an area equivalent to the area of that source. Accordingly, σ_Y in Eq. (S2.2a) can be modified as:

$$\sigma_Y = \sqrt{\left[\sigma_v t\left(1+\sqrt{\frac{t}{2T_Y}}\right)^{-1}\right]^2 + \left(\frac{d_s}{2}\right)^2} \tag{S2.3}$$

(b) Method-2: based on multiple point sources Gaussian simulations

As the above simple implementation of a Gaussian model for an area source dispersion in Method-1 is based on only the area of a source, it does not explicitly consider the geometry of an area source. In order to consider shape of an area source and also to test the above simple area source adaptation (Eq. (S2.3)) of the Gaussian model, we used another approach to model plume from an area source by decomposing the whole source area into multiple point sources. We discretizing a source region with a 2D grid with 5 m horizontal resolution. We considered each grid cell of the descretized area source as a point source with unitary emission rate and the plumes from these point sources were modelled using the Gaussian model (Eqs. (S2.1)-(S2.2)). These plumes from multiple point sources were superimposed to compute the averaged modelled plume from the area source at the measurement locations.

S2.2 Inversion procedure

S2.2.1 Characterization of the observation vector

As Gaussian plume models characterize a time averaged view of a plume, they cannot represent the observed instantaneous plume structure from the individual mobile plume cross-sections. Consequently, the emission estimates using the observed instantaneous CH_4 mole fractions can have a large uncertainty due to the different averaged and instantaneous nature of the respective modeled and observed CH_4 plumes. In order to limit the lack of simulation of the turbulent patterns using a Gaussian model, the integrals of the mole fractions above the background within cross-sections have been considered in different inversion approaches (Alberston et al., 2016; Ars et al., 2017, Kumar et al., 2021&2022). However, it is expected that a Gaussian plume model should appropriately represent an averaged observed plume computed using different plume cross-sections repeatedly conducted on the transects (described in section 2.3). Therefore, we defined an observation vector composed from the averaged CH_4 mole fractions computed from the different plume cross-sections at the locations with average distance between measurements. Since we have to estimate several sources of methane within the landfill site, following Ars et al. (2017), we divided the averaged CH_4 plume into several slices over space and a different observation vector is defined using the integrated CH_4 plumes in each slice. This approach reduces the tendency of the inversion to over-fit turbulent patterns within the plume.

Let $\boldsymbol{\mu} = (\mu_1, \mu_2, ...\mu_m)^T \in \mathbb{R}^m$ (superscript ^{T} defines the transpose of a vector/matrix) be the general notation for an observation vector containing m averages or slice-integrated values of the averaged CH_4 mole fractions, $\boldsymbol{\mu}_{pt}$ denotes an observation vector based on the averaged CH_4 mole fractions at the measurement locations and μ_{SI} denotes an observation vector based on the integrated CH_4 plumes in slices. We divide the plumes into different number of slices on ABC and EF roads with 50 m and 100 m distance intervals, respectively.

S2.2.2 The minimization process

The inversion process aims to minimize the root sum squared misfits between the averaged observed and modelled mole fraction enhancements in the plumes from the multiple potential sources. The inversions rely on a priori information about the potential emission sources (e.g., number, type, location, size and/or shape), $\boldsymbol{\mu}^{\mathbf{o}}$ as the measured observation vector, and the response functions h_{ij} simulated with the Gaussian plume model for the i^{th} measurement associated with the j^{th} potential emission source. For a multi-source inverse problem to estimate emission rates $\mathbf{q} = (q_1, q_2, ...q_p)^T$ of the p sources, simulations of the total modelled mole fractions above the background μ_i^{mod} at the i^{th} location from all the sources using Gaussian model is the sum of all the modelled mole fractions due to each of the p sources and can be computed by using h_{ij} as: $\mu_i^{mod} = \Sigma_{j=1}^{p} q_i h_{ij}$, or in matrix form:

$$\boldsymbol{\mu}^{\mathbf{mod}} = \mathbf{Hq} \tag{S2.4}$$

where $\boldsymbol{\mu}^{\mathbf{mod}} = (\mu_1^{mod}, \mu_2^{mod} ... \mu_m^{mod})^T$ is the modelled observation vector and $\mathbf{H}$ is the observation operator describing the atmospheric transport between the potential sources and the modeled mole fractions.

In order to estimate $\mathbf{q}$ using $\boldsymbol{\mu}^{\mathbf{o}}$ and $\boldsymbol{\mu}^{\mathbf{mod}}$, the inversion minimizes of the following cost function J:

$$J(\mathbf{q}) = \|\boldsymbol{\mu}^{\mathbf{o}} - \boldsymbol{\mu}^{\mathbf{mod}}\|^2 = \underset{\mathbf{q}\geq 0}{\operatorname{argmin}} \|\boldsymbol{\mu}^{o} - \mathbf{Hq}\|^2 \tag{S2.5}$$

Here $\|.\|$ denotes the Euclidean norm. Eq. (S2.5) can be solve for $\mathbf{q}$ using basic least-squares approach. However, the least-squares solution can lead to the negative emission estimates for some sources. In order to ensure $\mathbf{q} \geq 0$, we used non-negative least-squares (*nnls*) approach (Lawson and Hanson, 1995) for an approximate numerical solution of Eq. (S2.5) to estimate $\mathbf{q}$. A similar approach has been used to estimate methane emissions from a landfill in Figueroa et al. (2012)

S2.3 Inversion results from the selected campaigns

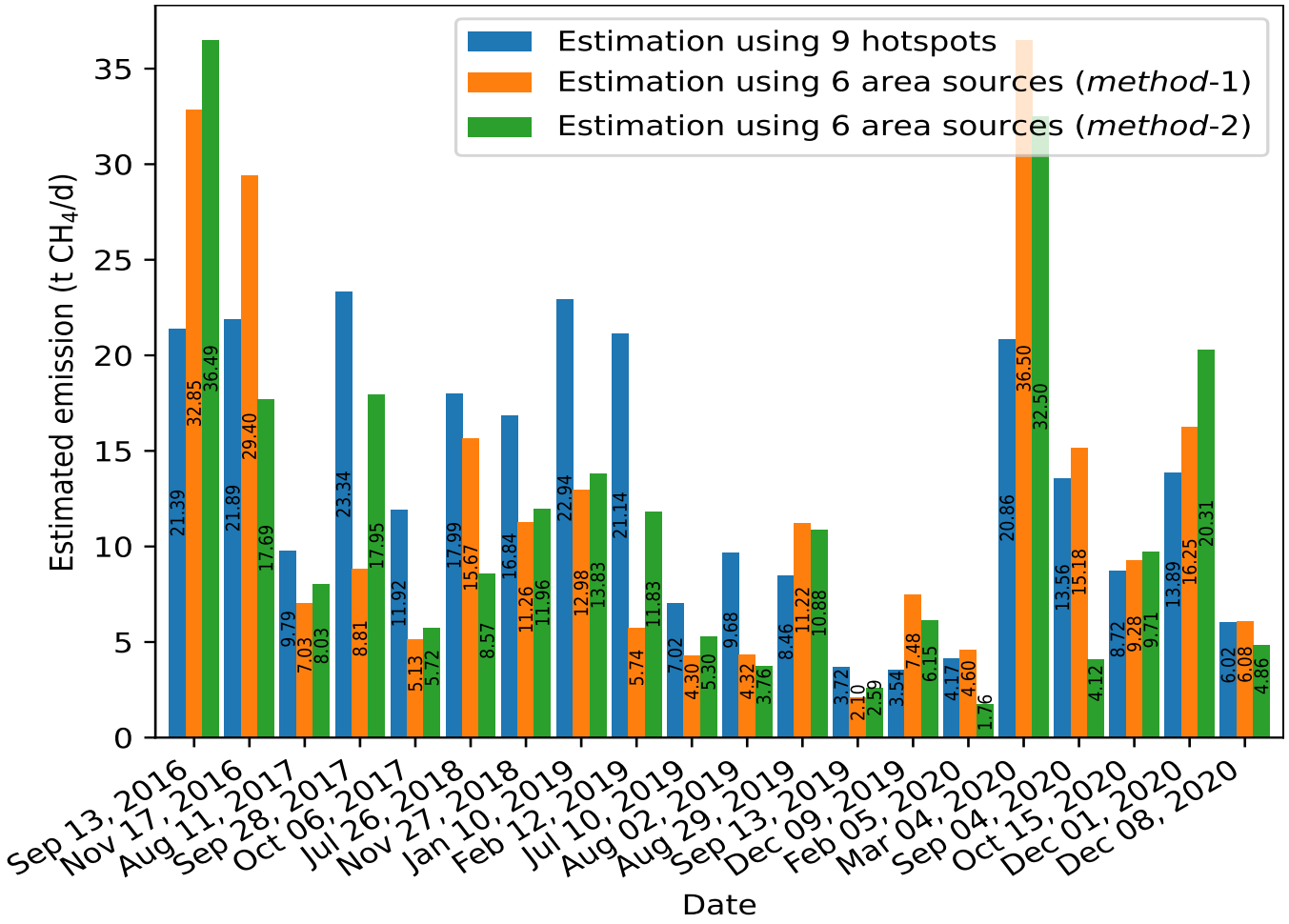

Figure S2.1. Summary of total estimated CH_4 emissions using 9 main hotspots from sniffing as point sources and 6 area sources (*method*-1: area source representation by modifying σ_Y from Eq. (1), *method*-2: area source representation by decomposing a source region into points) with observation vector μ_{pt} obtained from the measurements along the ABC road.

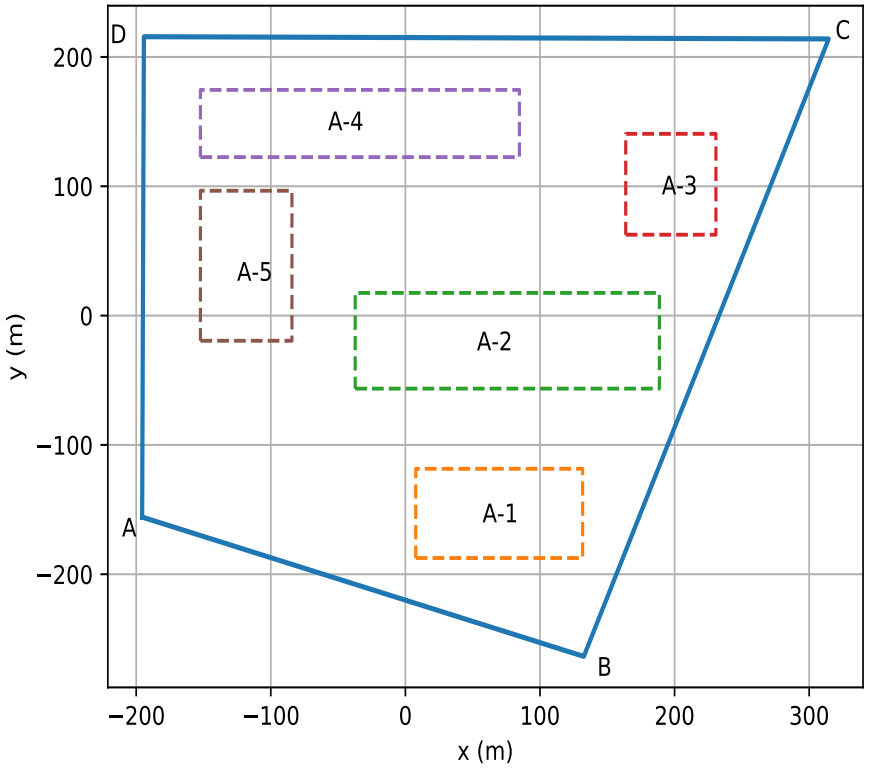

Figure S2.2. Five potential area sources (rectangular boxes, A-i, i=1,..,5) on the Butte-Bellot landfill defined by Albergel et al. (2017).

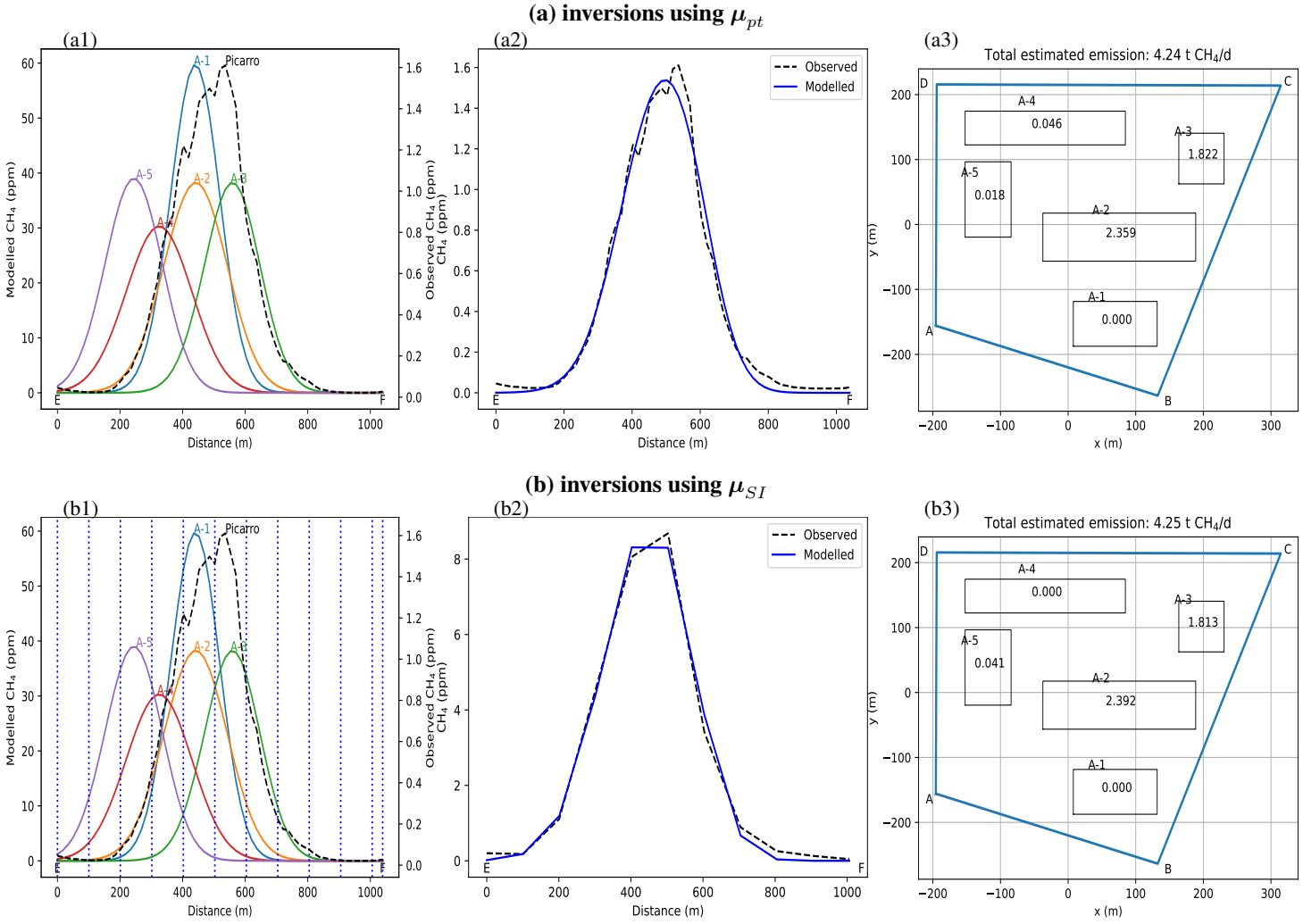

Figure S2.3. Modelling the individual plumes and emissions from the inversion tests using five potential area sources (Figure S2.2) with two observation vectors (a) $\boldsymbol{\mu}_{pt}$(first row) and (b) $\boldsymbol{\mu}_{SI}$(second row) obtained from the EF measurements from the campaign on **January 10, 2019**. From left to right in each row, first to third columns plots respectively show the average CH_4 mole fraction enhancements above the background measured (black dashed line, right Y-axis) and modelled response functions (solid coloured lines, left Y-axis), the fit between the observed (black dashed line) and modelled (blue sold line) CH_4 mole fraction enhancements along the measurement path, and the estimates of the methane emissions for each source. Vertical black dotted lines in second row's first column figure show the point of division of the road into sub-segment over which the mole fractions are integrated to define $\boldsymbol{\mu}_{SI}$.

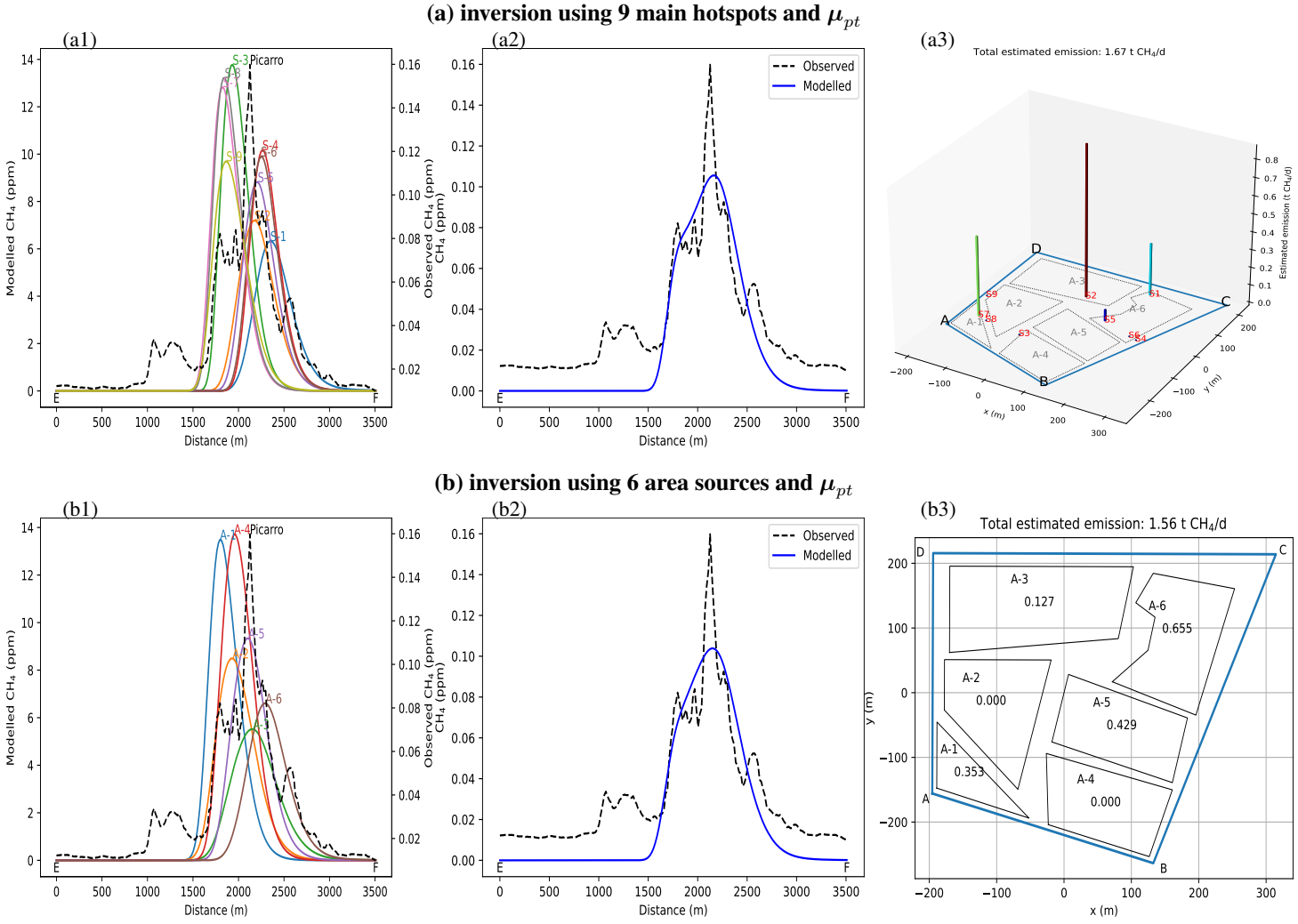

Figure S2.4. Modelling the individual plumes and emission rates from the inversion tests using (a) 9 main hotspots and (b) six area sources for $\boldsymbol{\mu}_{pt}$ from the measurements obtained along the EF road on **August 11, 2017**. From left to right in each row, first to third columns plots respectively show the average CH_4 mole fraction enhancements above the background (black dashed line, right Y-axis) and the modelled response functions (solid colored lines for *method*-1 and the same colored dotted lines for *method*-2, left Y-axis) for each potential sources, the fit between the observed (black dashed lines) and modelled (blue sold lines) CH_4 mole fraction enhancements, and estimates of the CH_4 emissions (t CH_4 /d) for each of the potential sources.

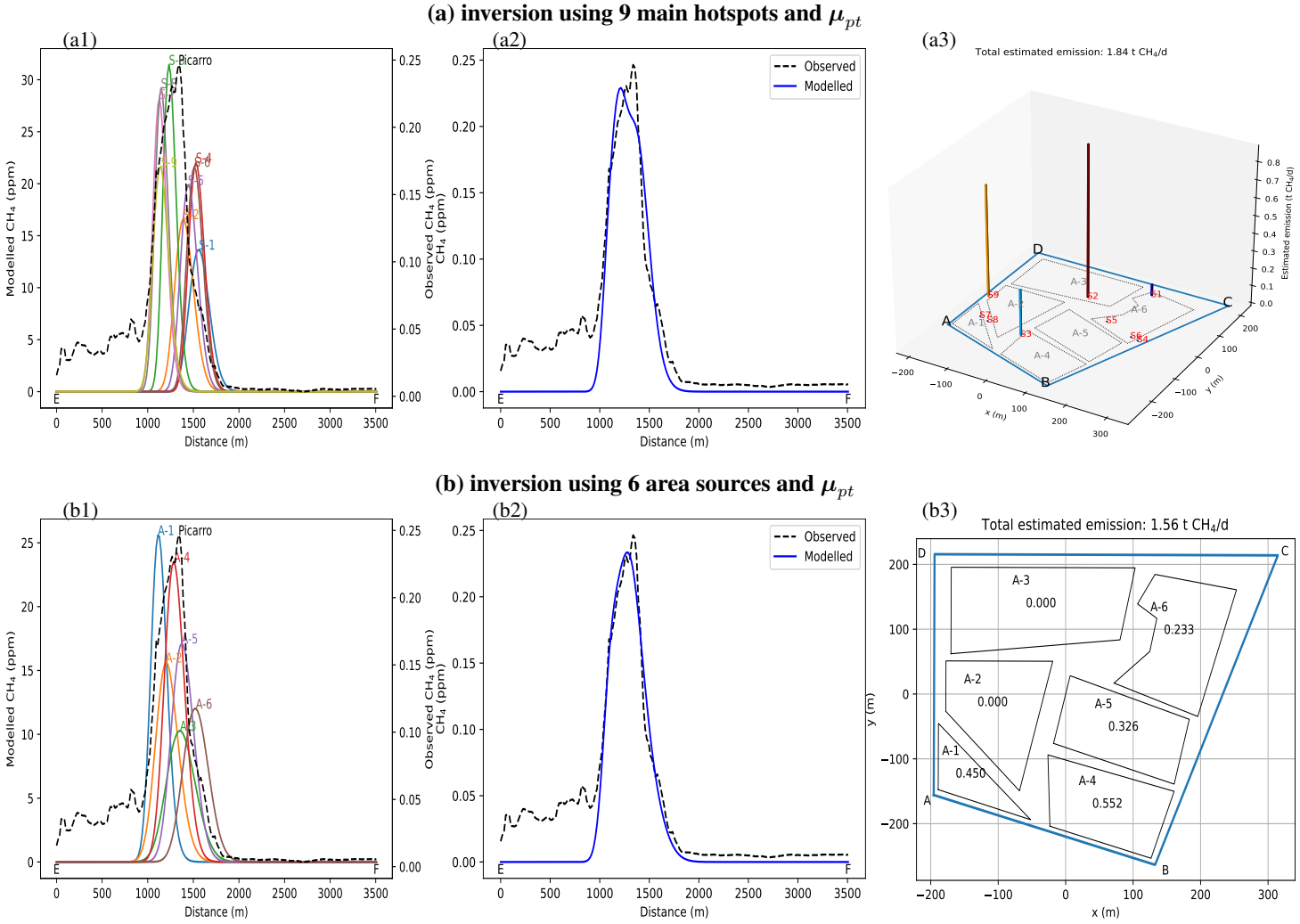

Figure S2.5. Same as Figure S2.4, but for the measurements obtained along the EF road on **October 06, 2017**.

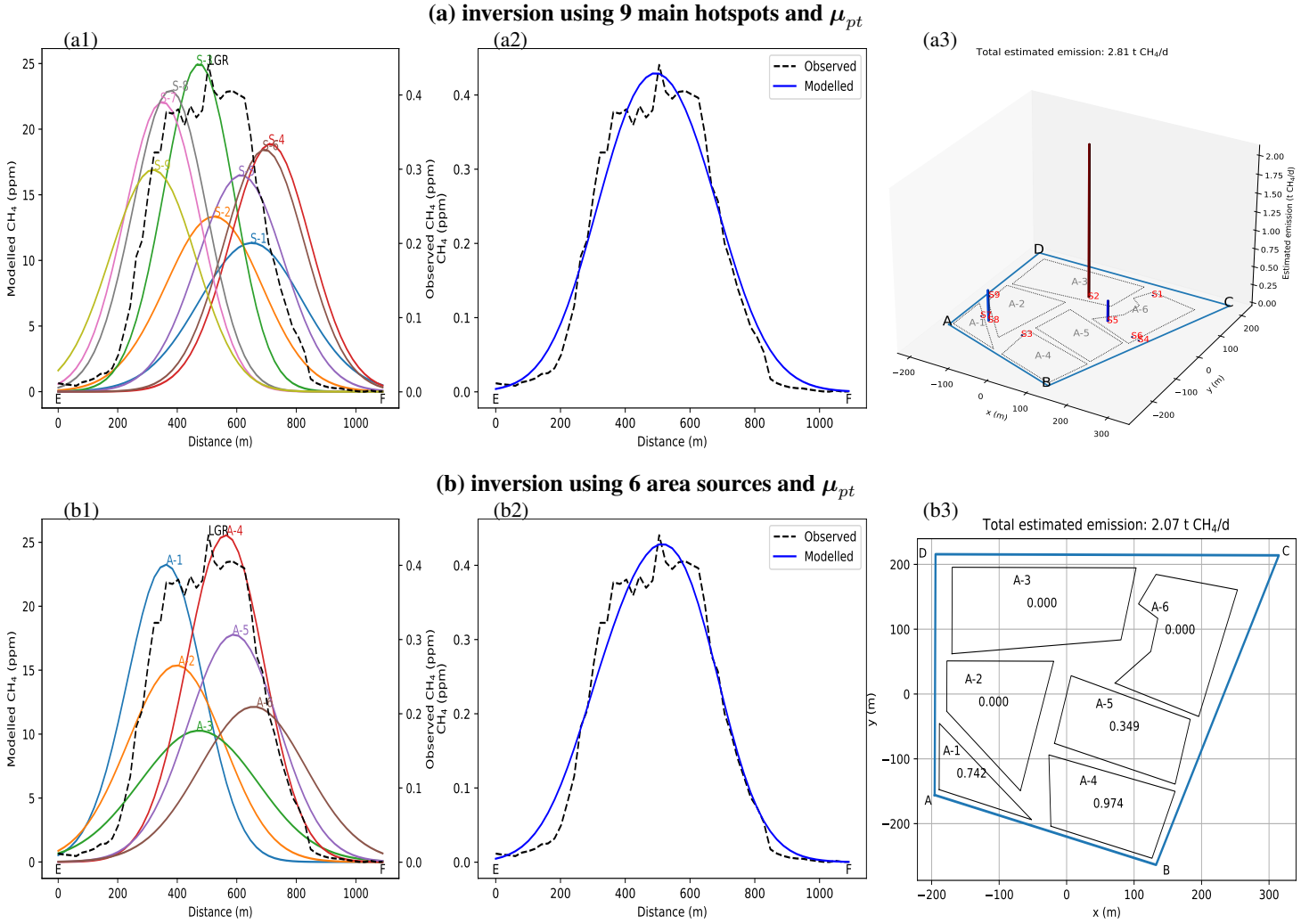

Figure S2.6. Same as Figure S2.4, but for the measurements obtained along the EF road on **July 26, 2018**.

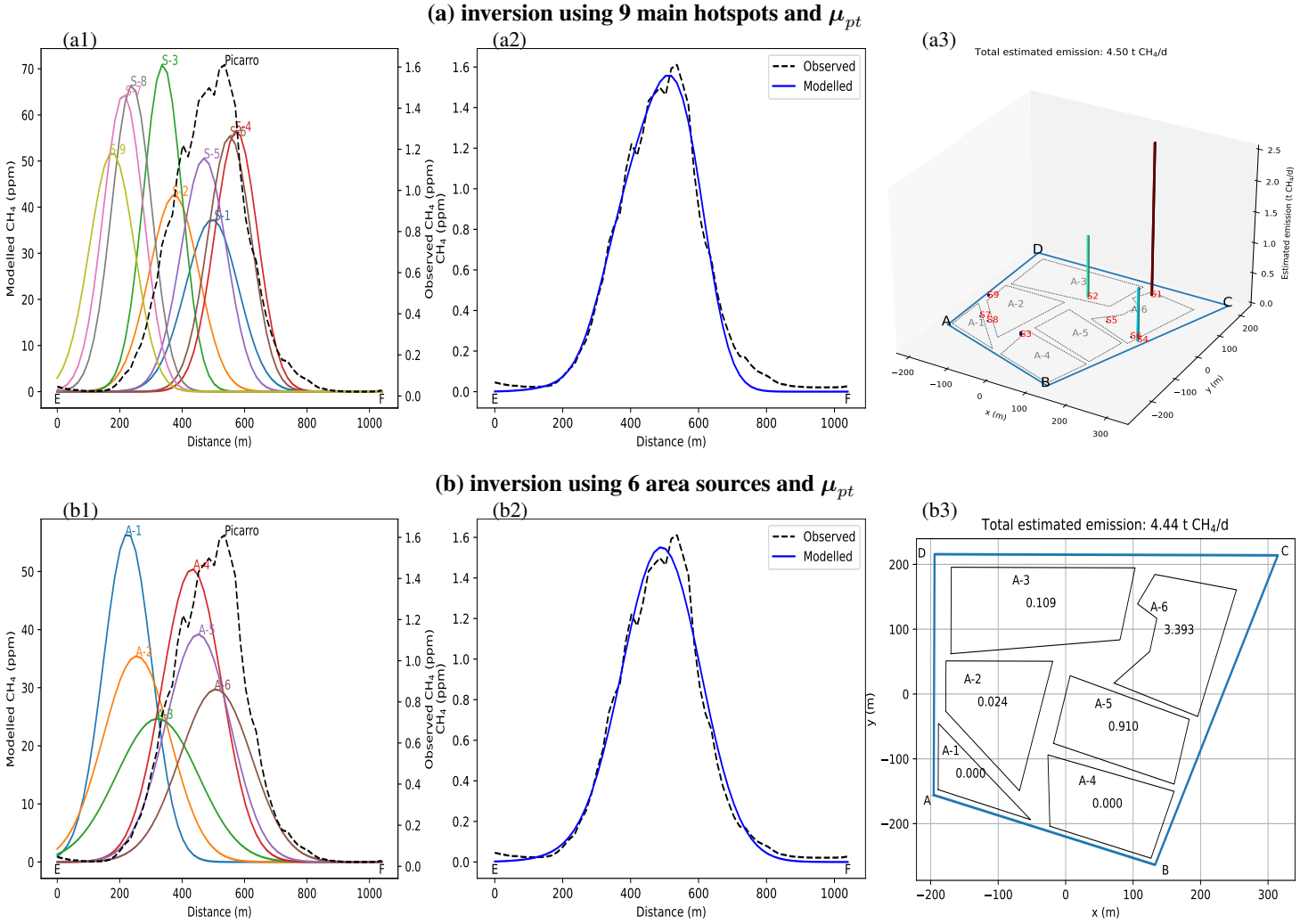

Figure S2.7. Same as Figure S2.4, but for the measurements obtained along the EF road on **January 10, 2019**.

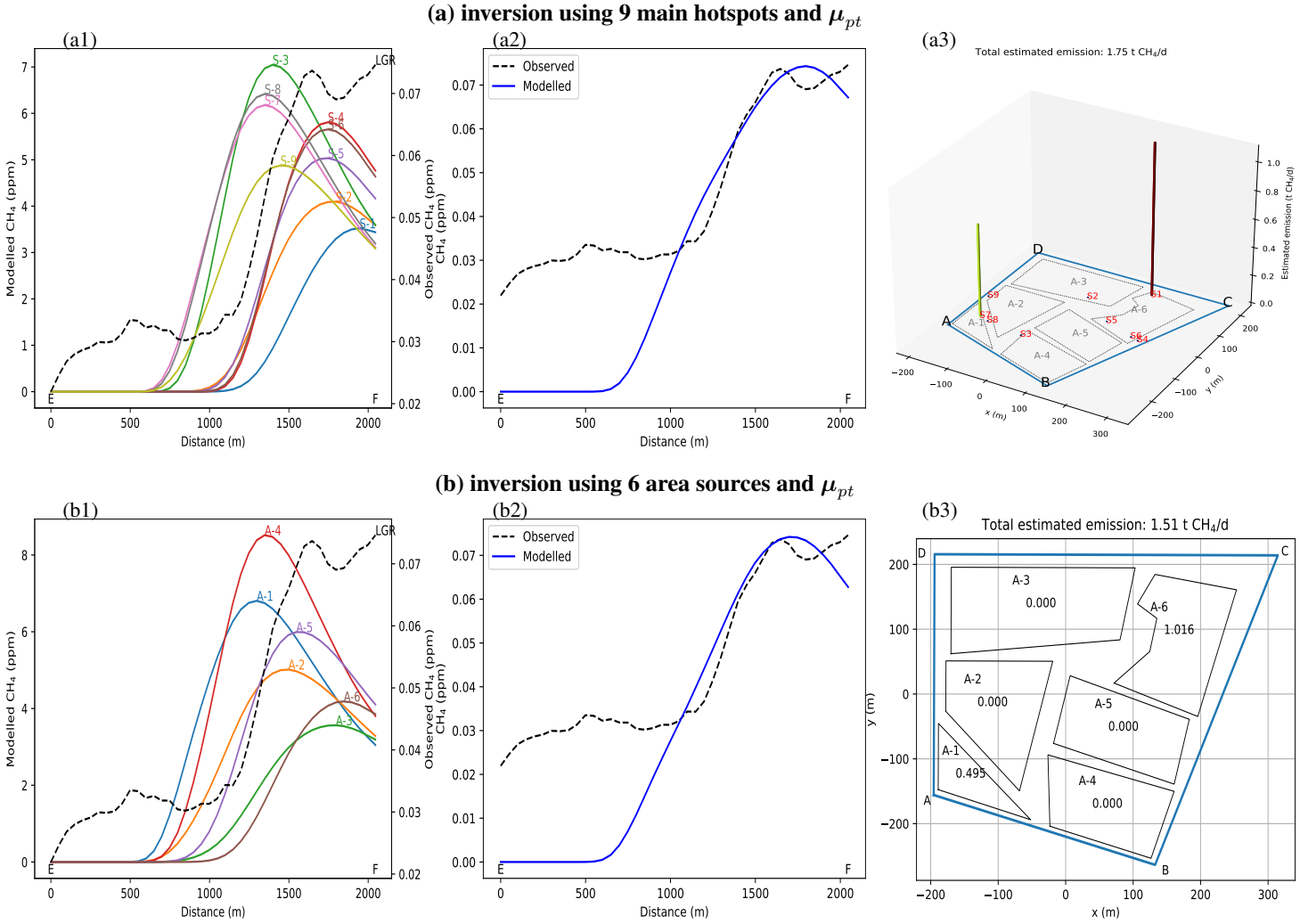

Figure S2.8. Same as Figure S2.4, but for the measurements obtained along the EF road on **February 12, 2019**.

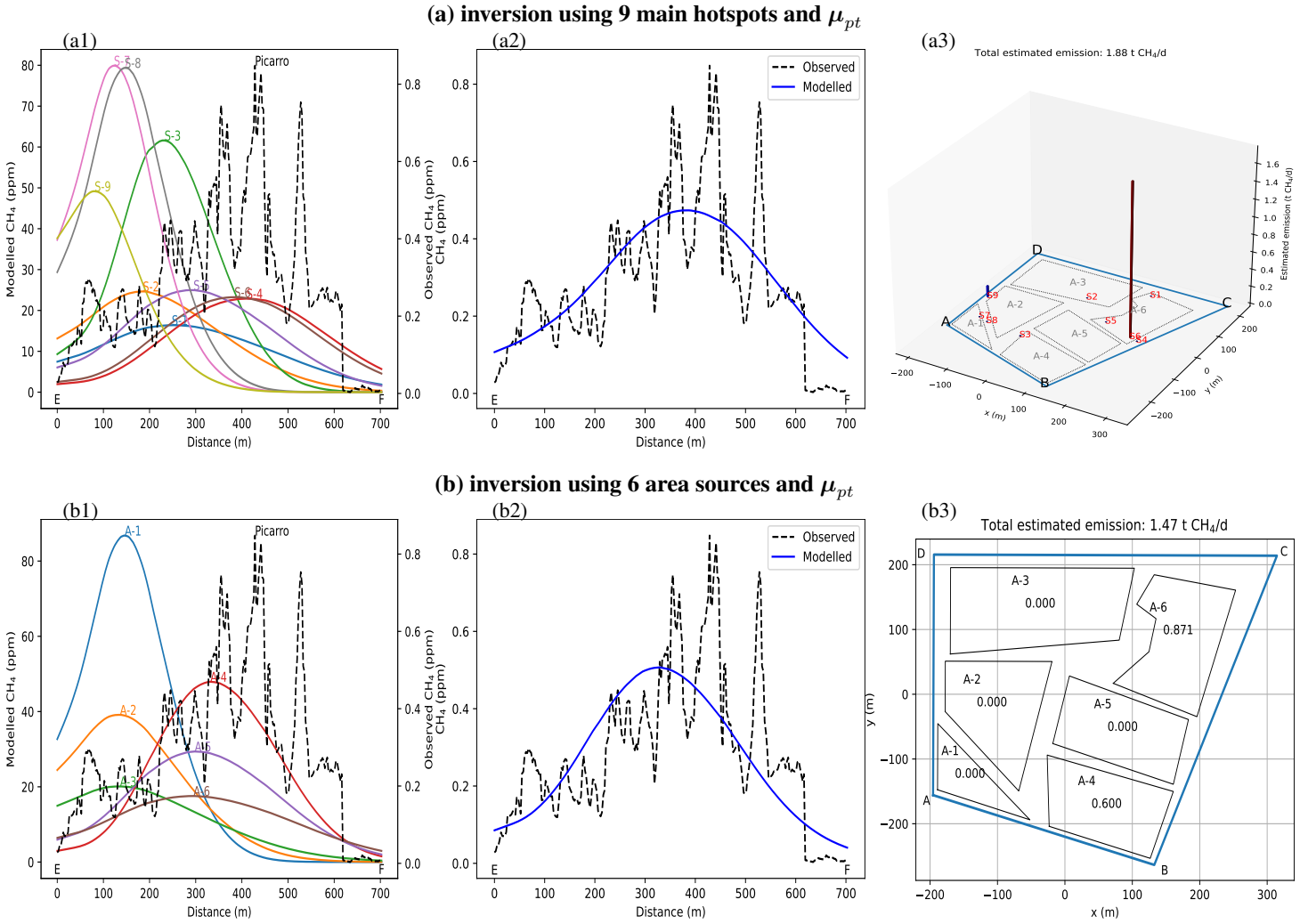

Figure S2.9. Same as Figure S2.4, but for the measurements obtained along the EF road on **July 10, 2019**.

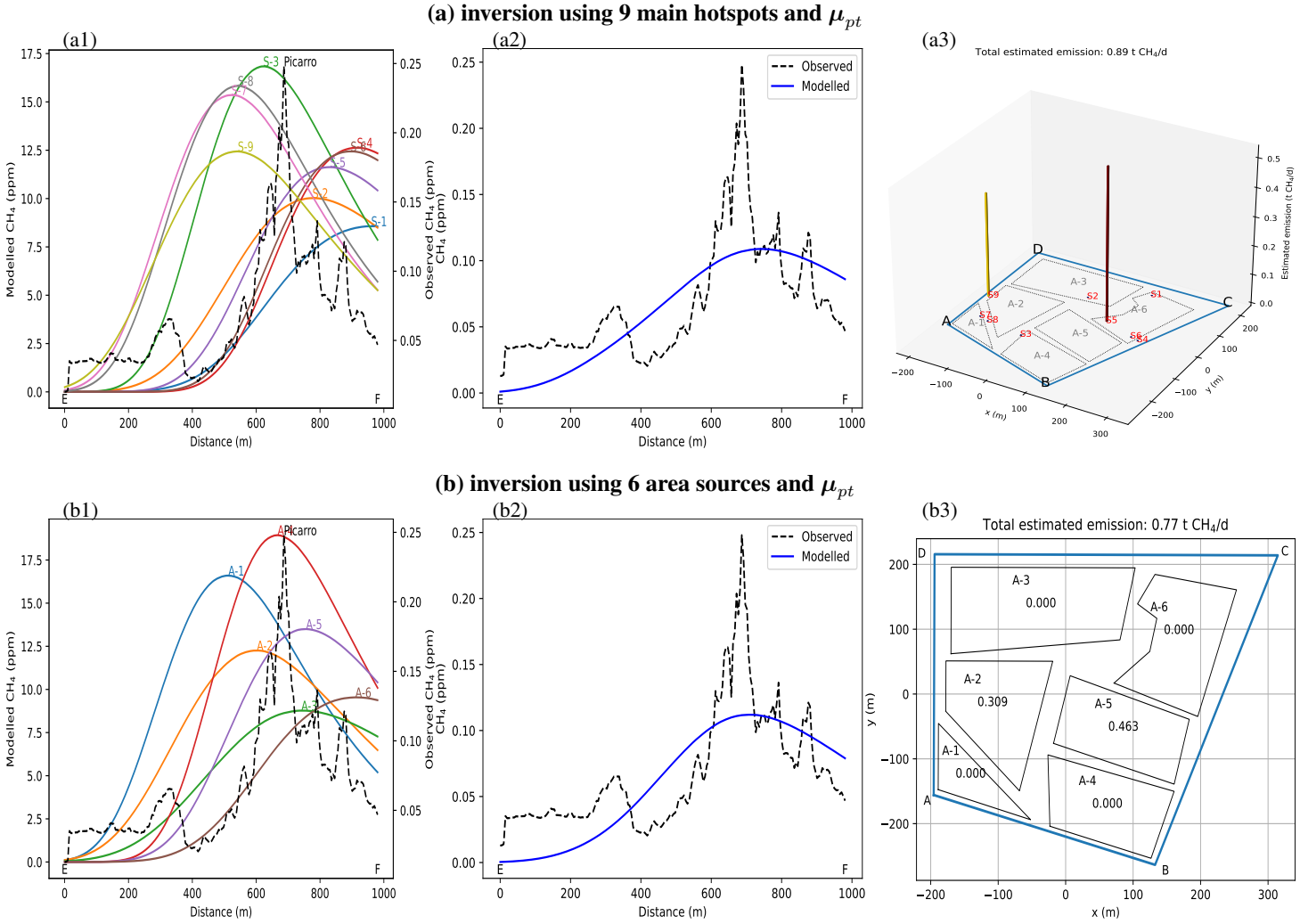

Figure S2.10. Same as Figure S2.4, but for the measurements obtained along the EF road on **August 02, 2019**.

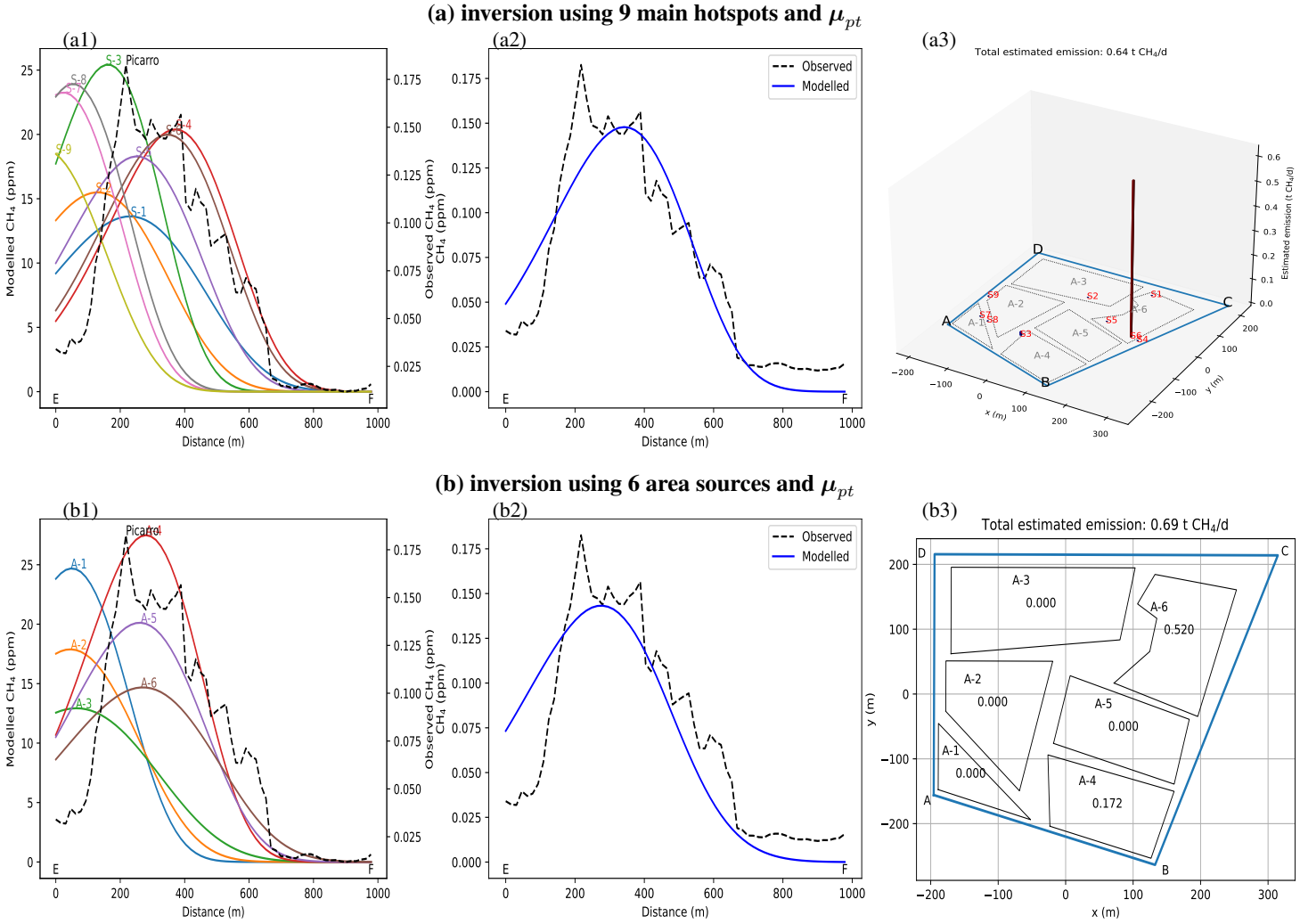

Figure S2.11. Same as Figure S2.4, but for the measurements obtained along the EF road on **September 13, 2019**.

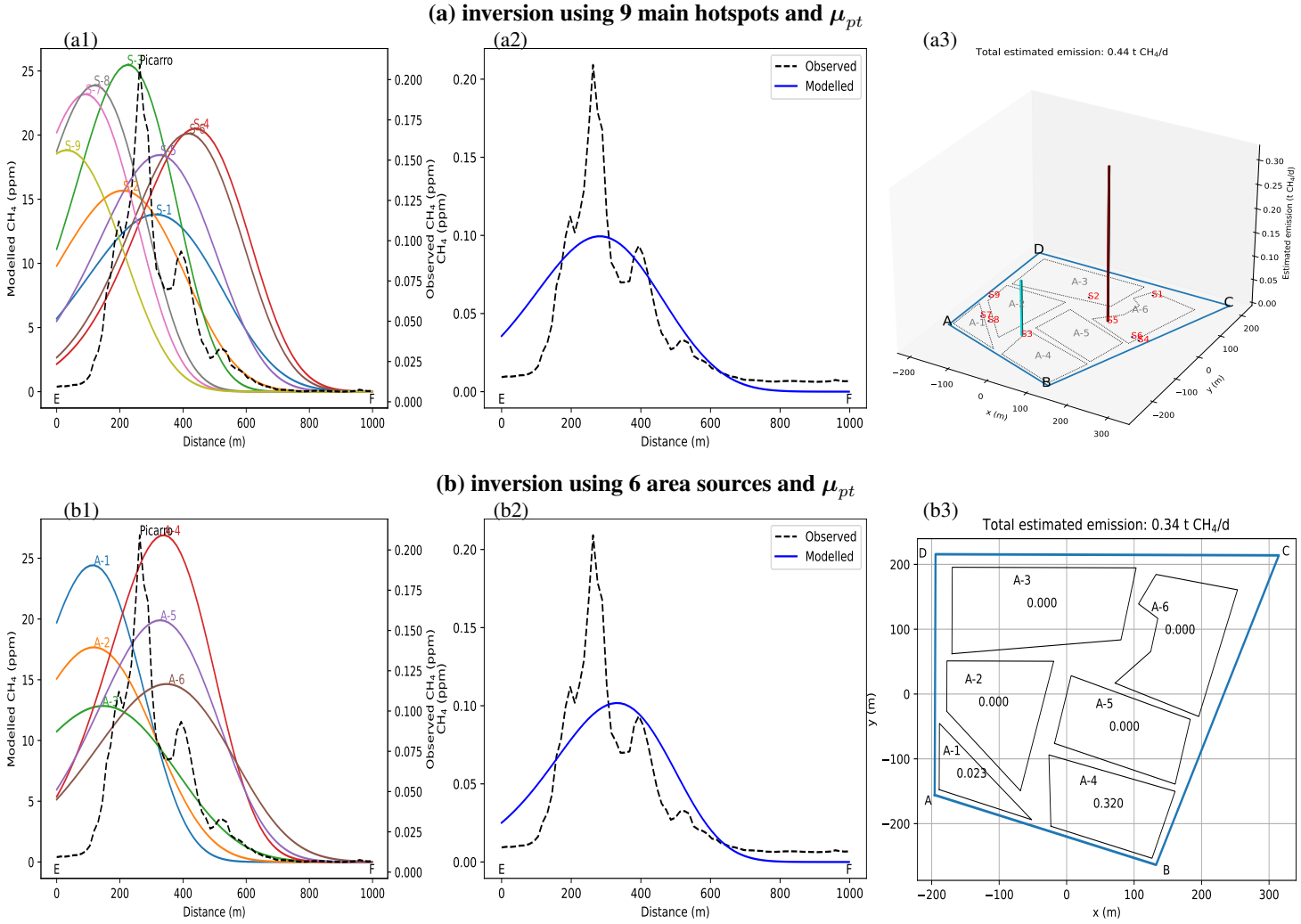

Figure S2.12. Same as Figure S2.4, but for the measurements obtained along the EF road on **February 05, 2020**.

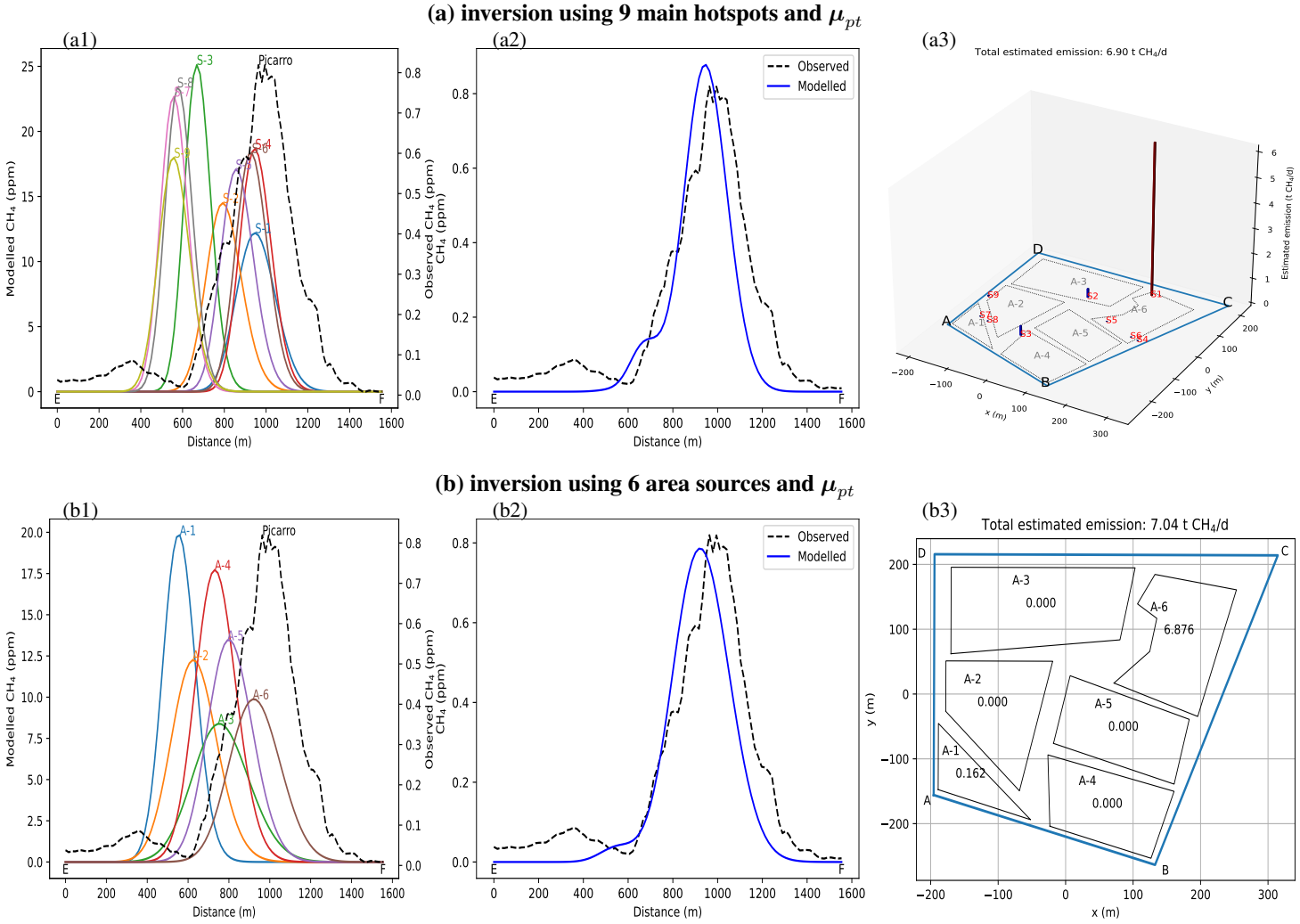

Figure S2.13. Same as Figure S2.4, but for the measurements obtained along the EF road on **December 01, 2020**.

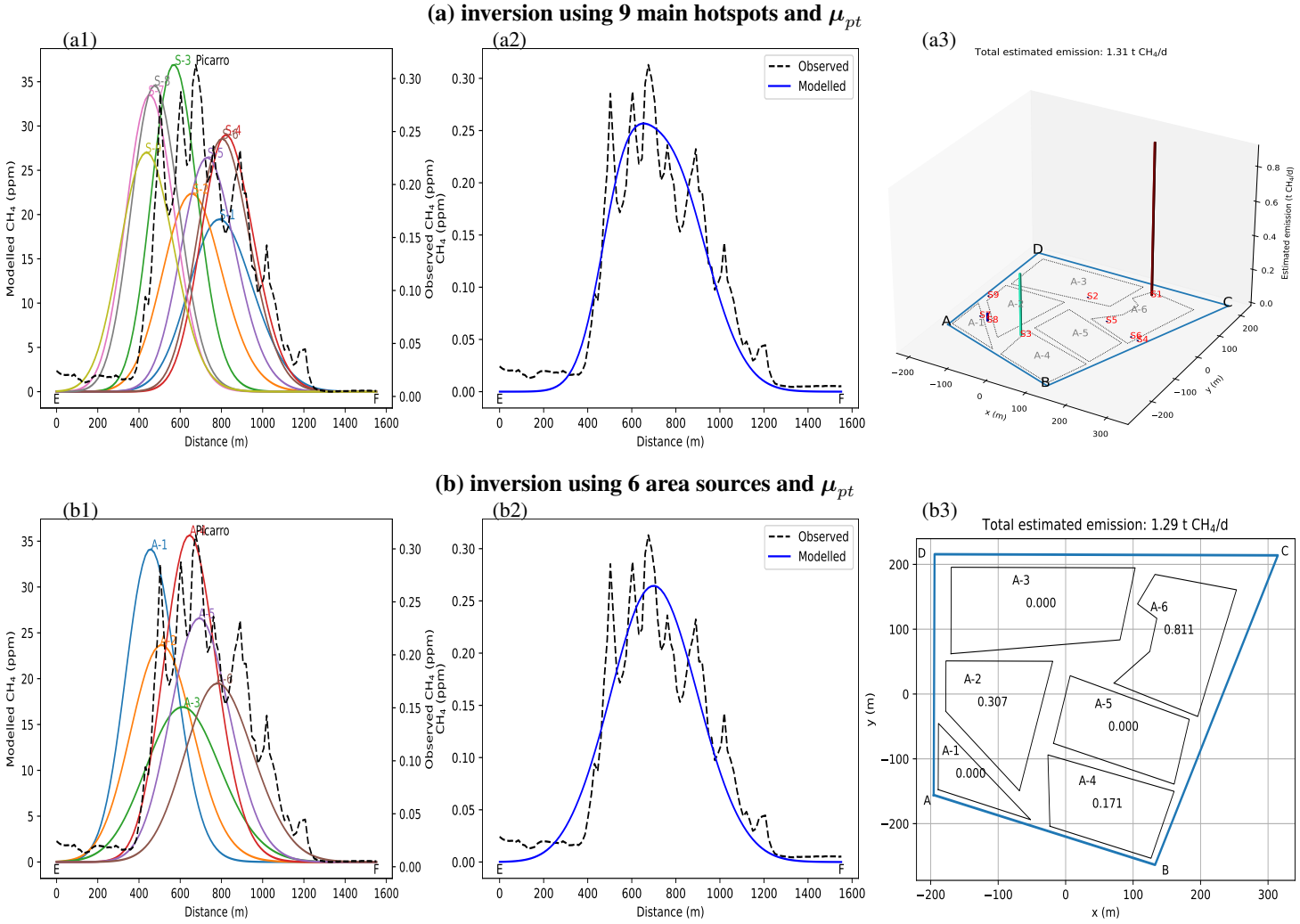

Figure S2.14. Same as Figure S2.4, but for the measurements obtained along the EF road on **December 08, 2020**.

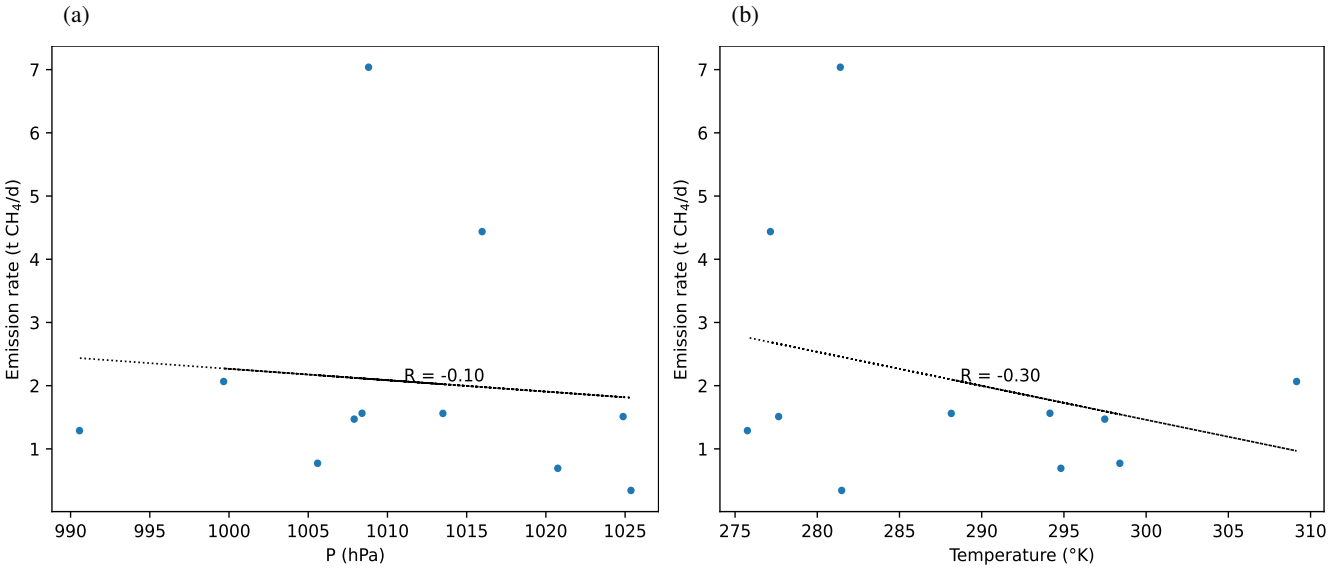

Figure S2.15. Estimated CH_4 emissions using EF measurements as a function of (a) atmospheric pressure and (b) atmospheric temperature.

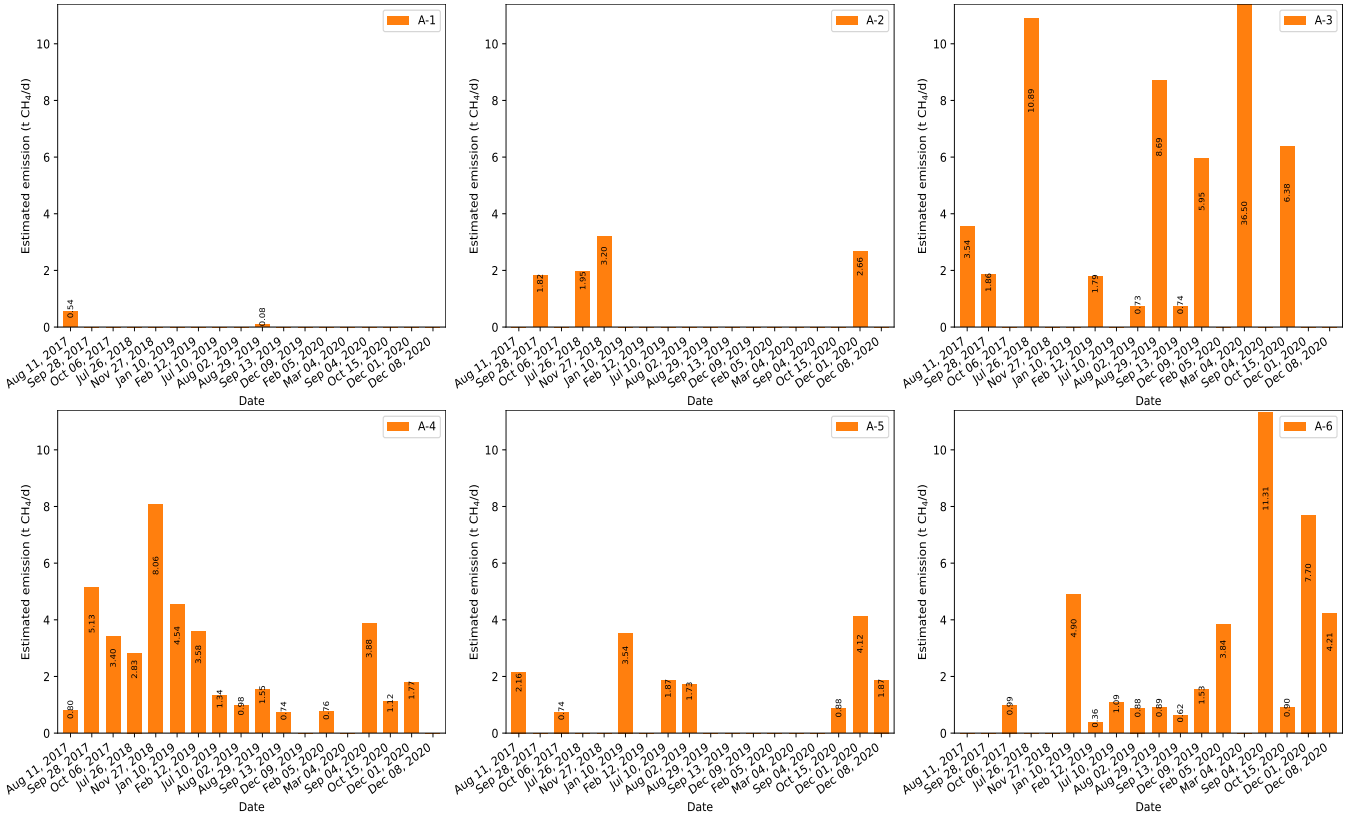

Figure S2.16. Summary of the estimated CH_4 emissions in each source region using six area sources (*method*-1) with observation vector $\boldsymbol{\mu}_{pt}$ obtained from the measurements along the ABC road.

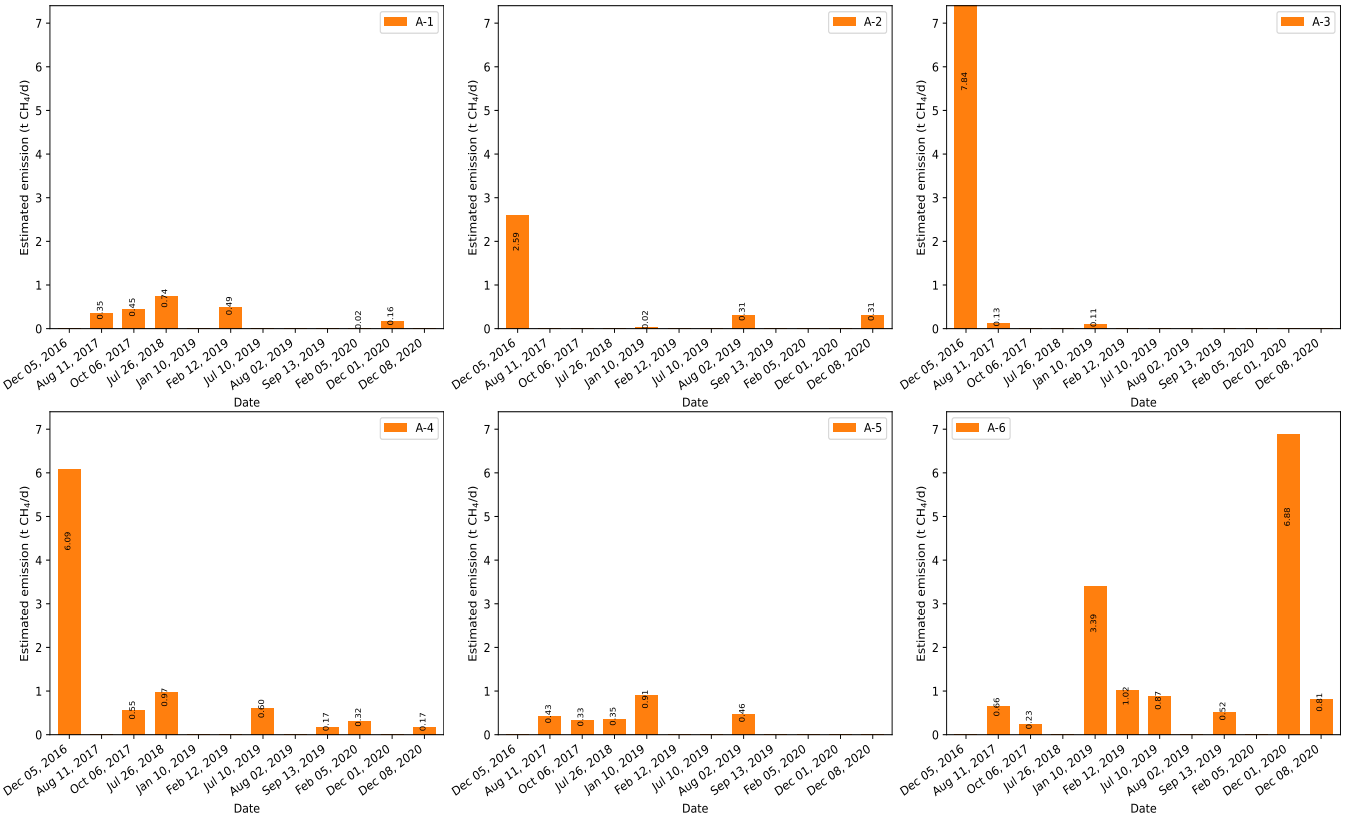

Figure S2.17. Summary of the estimated CH_4 emissions in each source region using six area sources (*method*-1) with observation vector $\boldsymbol{\mu}_{pt}$ obtained from the measurements along the EF road.

References

Briggs, G.A., 1973. Diffusion estimation for small emissions. Atmospheric turbulence and diffusion laboratory 965, 83–145.

Draxler, R., 1976. Determination of atmospheric diffusion parameters. Atmospheric Environment (1967) 10, 99–105. URL: https://www.sciencedirect.com/science/article/pii/0004698176902262, doi:https://doi.org/https://doi.org/10.1016/0004-6981(76)90226-2.

Gryning, S., Holtslag, A., Irwin, J., Sivertsen, B., 1987. Applied dispersion modelling based on meteorological scaling parameters. Atmospheric Environment (1967) 21, 79–89. URL: https://www.sciencedirect.com/science/article/pii/0004698187902733, doi:https://doi.org/https://doi.org/10.1016/0004-6981(87)90273-3.

Korsakissok, I., Mallet, V., 2009. Comparative study of gaussian dispersion formulas within the polyphemus platform: evaluation with prairie grass and kincaid experiments. Journal of applied meteorology and climatology 48, 2459–2473.